Uncertainty quantification of time-average quantities of chaotic systems using sensitivity-enhanced polynomial chaos expansion

Kyriakos D. Kantarakias* and George Papadakis†
Department of Aeronautics, Imperial College London, London SW7 2AZ, United Kingdom

(Received 28 October 2023; accepted 19 March 2024; published 12 April 2024)

We consider the effect of multiple stochastic parameters on the time-average quantities of chaotic systems. We employ the recently proposed sensitivity-enhanced generalized polynomial chaos expansion, se-gPC, to quantify efficiently this effect. se-gPC is an extension of gPC expansion, enriched with the sensitivity of the time-averaged quantities with respect to the stochastic variables. To compute these sensitivities, the adjoint of the shadowing operator is derived in the frequency domain. Coupling the adjoint operator with gPC provides an efficient uncertainty quantification algorithm, which, in its simplest form, has computational cost that is independent of the number of random variables. The method is applied to the Kuramoto-Sivashinsky equation and is found to produce results that match very well with Monte Carlo simulations. The efficiency of the proposed method significantly outperforms sparse-grid approaches, such as Smolyak quadrature. These properties make the method suitable for application to other dynamical systems with many stochastic parameters.

DOI: 10.1103/PhysRevE.109.044208

I. INTRODUCTION

The performance of real-world systems is significantly affected by the uncertainty of the parameters that define these systems. Large research effort has focused on the quantification of the effect of such stochastic variations to a quantity of interest (QoI), usually a time-averaged quantity. This field of research is commonly known as uncertainty quantification (UQ) and efficient UQ methods have been developed for static and dynamic problems [1–4].

In the standard generalized polynomial chaos (gPC) method, originally proposed in Refs. [2,5], an orthonormal polynomial base that spans the stochastic space is used for the spectral representation of uncertain quantities. The spectral coefficients are computed with Galerkin projection, allowing for the efficient evaluation of the statistics of the QoI. However, the cost of gPC scales as $\sim m^p$, where m is the number of stochastic parameters and p the polynomial order of the expansion. This exponential growth is known as the curse of dimensionality [3]. Various approaches have been proposed to mitigate the rapid growth of the computational cost, such as sparse grid approaches such as Smolyak grids [6], or adaptive methods that build a sparse polynomial chaos expansion (PCE) basis using least-angle regression [7]. gPC methods have been successful in predicting the statistics of the QoI in many applications, such as fluid dynamics, mechanics, space, medicine, see, for example, Refs. [2,4,8–10]. Applications of gPC to chaotic systems have also appeared in the literature [11–15].

Another method for the computation of the spectral coefficients is based on the least-squares approach [3,16]. To reduce the computational coast, the method is usually coupled with efficient multidimensional sampling techniques; for an overview of the different sampling algorithms, see Ref. [17]. Recently, new sampling approaches that incorporate real-world data into the computation of the gPC coefficients have been introduced [18–20]. However the cost still grows exponentially with the number of uncertain parameters, making such methods difficult to apply in systems with a large m.

In this paper we use the sensitivity-enhanced gPC, or se-gPC, a least-squares approach for the computation of the spectral coefficients that is augmented with the sensitivity of the QoI with respect to the uncertain parameters, see Ref. [21] for a detailed description of the method and a review of previous works in this area. When all the sensitivities are computed efficiently in a single step with the adjoint method, the computational cost of se-gPC is reduced by a factor m, i.e., it scales as $\sim m^{p-1}$, and the method becomes increasingly useful as the number of stochastic inputs grows. Efficient sampling algorithms can by employed to reduce the number of required evaluations, see Ref. [21] for comparison between two such algorithms. For the special case of first-order spectral representation, i.e., for $p = 1$, the spectral coefficients can be estimated with a single direct and a single adjoint evaluation, regardless of the number of stochastic inputs.

The se-gPC is efficient because the sensitivities of the QoI with respect to all stochastic inputs at one sampling point can be estimated using a single adjoint evaluation. Adjoint methods have long been successfully used to estimate derivatives (sensitivities) for stationary or nonchaotic systems in aerodynamics [22], structural optimization [23], chemical

*k.kantarakias@imperial.ac.uk
†g.papadakis@imperial.ac.uk

Published by the American Physical Society under the terms of the Creative Commons Attribution 4.0 International license. Further distribution of this work must maintain attribution to the author(s) and the published article's title, journal citation, and DOI.

kinetic systems [24], among many others. However, when the underlying system is chaotic, a small variation in an input parameter causes large deviation in the trajectory of the system in phase space (with respect to the reference trajectory); this is popularly known as butterfly effect. Under these circumstances, standard sensitivity analysis tools (such as adjoint) fail to produce physically meaningful results [25,26]. Mathematically, the deviation between the two trajectories is due to the presence of one or more positive Lyapunov exponents. To address this problem, the least-squares shadowing (LSS) method and its variants were proposed in a series of papers [27–29]. This method relies on the shadowing lemma [30,31] and provides a systematic and rigorous approach for the computation of sensitivities of time-average quantities of chaotic systems.

Assume a reference trajectory of a dynamical system evaluated for a parameter value s, $\boldsymbol{u}(t;s)$. Shadowing methods aim to compute another trajectory at $s+\delta s$, $\boldsymbol{u}(\tau; s+\delta s)$ that shadows, or stays close to, the reference trajectory for the time frame T of the analysis. The sensitivity problem is reformulated as a minimization problem between the reference and the shadowing trajectories. The solution results in two trajectories that remain close to each other, and can be used to compute accurate sensitivities for a long T. Note that the two trajectories start from different initial conditions, but for ergodic systems this does not affect the time-average QoI. Also, the time variable in the shadowing trajectory is not be the same as t, thus a different symbol, τ, is used.

Various approaches have been proposed to improve the computational efficiency of the original LSS method. The multiple shooting shadowing (MSS) algorithm [32] was introduced to reduce the memory requirements of the standard LSS. When coupled with a matrix-free preconditioner to improve the convergence rate [33], MSS has lower computational cost and memory requirements than standard LSS. In Ref. [34], the nonintrusive LSS (NILSS) approach was derived and applied successfully to the two-dimensional (2D) flow over a backward facing step and later to 3D flows inside a channel and around a cylinder [35,36]. The computational cost of NILSS methods scales linearly with the number of positive Lyapunov exponents (PLEs). Theoretical predictions indicate that the highest Lyapunov exponent scales with the inverse of the Kolmogorov time scale [37,38]. Yet another approach is the formulation of the shadowing problem in the frequency domain; to this end, the shadowing harmonic operator was introduced recently [39]. The cost of the method is case dependent, but for the Kuramoto-Sivashinsky system, sensitivities are computed at a cost roughly equal to that of the baseline solution.

In this paper, we derive the adjoint of the shadowing harmonic operator. The adjoint formulation allows us to compute the sensitivity of a time-average QoI of a chaotic dynamical system with respect to multiple parameters at a cost independent of the number of parameters. These sensitivities are then used to compute the UQ spectral coefficients in the context of se-gPC. As mentioned earlier, for spectral order $p=1$, the cost of se-gPC is independent of m. This is an application of UQ in chaotic systems with computational cost independent of the number of stochastic parameters. The method is applied and tested to the stochastically forced Kuramoto-Sivashinski equation and the results are compared against reference data obtained from Monte Carlo simulations.

The rest of this paper is structured as follows. In Sec. II an overview of the standard gPC and se-gPC formulations is given. The adjoint shadowing harmonic operator for a general dynamical system is derived in Sec. III. The se-gPC is applied to the Kuramoto-Sivashinsky equation with a single and multiple uncertain forcing parameters in Secs. IV and V, respectively. Finally, in Sec. VI the main findings of the paper are summarized.

II. SENSITIVITY-ENHANCED UNCERTAINTY QUANTIFICATION

Consider a dynamical system governed by a set of ordinary differential equations,

$$\frac{d\boldsymbol{u}}{dt} = f(\boldsymbol{u};\boldsymbol{s})$$
$$\boldsymbol{u}(0;\boldsymbol{s}) = \boldsymbol{u}_0(\boldsymbol{s}), \tag{1}$$

where $\boldsymbol{u}(t;\boldsymbol{s}) \in \mathbb{R}^{N_u}$ is the vector of state variables and $\boldsymbol{s} \in \mathbb{R}^{N_s}$ is a set of control parameters that define the dynamics of the system (for example Reynolds number in the case of incompressible fluid flows). We assume that the vector field $\boldsymbol{f} : \mathbb{R}^{N_u} \times \mathbb{R}^{N_s} \to \mathbb{R}^{N_u}$ varies smoothly with $\boldsymbol{u}$ and $\boldsymbol{s}$. In most practical applications, we are interested in a time-averaged quantity $\overline{J}(\boldsymbol{s}) : \mathbb{R}^{N_s} \to \mathbb{R}$,

$$\overline{J}(\boldsymbol{s}) = \lim_{T\to\infty} \frac{1}{T}\int_0^T J(\boldsymbol{u},\boldsymbol{s})dt, \tag{2}$$

which is usually referred to as the quantity of interest (QoI), for example mean lift or drag coefficient of an aerofoil. We assume that the control parameters $\boldsymbol{s}$ are functions of m independent stochastic variables ξ_i that form the vector $\boldsymbol{\xi} = [\xi_1, \ldots, \xi_m]$. Each random variable ξ_i is characterized by a probability density function (PDF), $w_i(\xi_i)$ in the domain $\mathcal{E}_i$. We seek to estimate the effect of $\boldsymbol{\xi}$ on the statistics of $\overline{J}(\boldsymbol{s})$.

This effect can be quantified via the generalized polynomial chaos (gPC) expansion. In gPC a complete probability space $\mathbb{P} = (\Omega, \Sigma, d\mathcal{P})$ is defined, where Ω refers to the set of random events and the probability measure $d\mathcal{P}$ is characterized by the σ algebra Σ. The vector $\boldsymbol{\xi}$ follows the PDF $W = \prod_{i=1}^m w_i(\xi_i)$, defined in the domain $\mathcal{E} = \prod_{i=1}^m \mathcal{E}_i$. This stochastic space is spanned by a polynomial basis $\Psi = \{\Psi_0, \Psi_1, \ldots\}$, which is orthogonal to W with respect to the inner product,

$$\langle \Psi_j, \Psi_k \rangle = \int_{\mathcal{E}} \Psi_j W \Psi_k d\boldsymbol{\xi} = \delta_{jk}\langle \Psi_j, \Psi_j \rangle. \tag{3}$$

The polynomial basis is normalized so that $\langle \Psi_j, \Psi_j \rangle = 1$. When $m > 1$, Ψ is defined by the tensor product of the unitary polynomials $\psi^{(i)}$, as in $\Psi := \otimes_{i=1}^m \psi^{(i)} = \{\Psi_0, \Psi_1, \ldots\}$. The base is truncated to a finite number of polynomials by limiting the order of Ψ_j to p. In that case, the QoI $\overline{J}$ is written in spectral form as

$$\overline{J}(\boldsymbol{\xi}) = \sum_{i=0}^{P} c^{(i)}\Psi_i(\boldsymbol{\xi}) + \boldsymbol{\epsilon}(\boldsymbol{\xi}), \tag{4}$$

where the number of basis functions is given by,

$$P+1=\frac{(p+m)!}{p!m!}, \tag{5}$$

and $\boldsymbol{\epsilon}(\boldsymbol{\xi})$ is the truncation error (due to finite P). In UQ with gPC, the goal is to compute the spectral coefficients $c^{(i)}$ in a computationally efficient manner. The statistical moments of $\overline{J}(\boldsymbol{\xi})$ can be easily computed algebraically from $c^{(i)}$, see Eq. (5) in Ref. [21].

In this paper, the coefficients are computed via a weighted least-squares (WLS) approach. To this end, q realizations of $\boldsymbol{\xi}$ are defined, with the ith realization written as $\boldsymbol{\xi}^{(i)}=[\xi_1^{(i)},\ldots,\xi_m^{(i)}]$. The QoI $\overline{J}$ is computed for q realizations and stored in the vector $\mathbf{Q}=[\overline{J}(\boldsymbol{\xi}^{(1)}),\ldots,\overline{J}(\boldsymbol{\xi}^{(q)})]^\top$. Defining the vector $\boldsymbol{c}=[c^{(0)},\ldots,c^{(P)}]^\top\in\mathbb{R}^{P+1}$, Eq. (4) can be written in matrix form as,

$$\mathbf{Q}=\boldsymbol{\psi}\boldsymbol{c}+\boldsymbol{\epsilon}, \tag{6}$$

where $\boldsymbol{\psi}$ is the measurement matrix with elements $\boldsymbol{\psi}_{ij}=\Psi_j(\boldsymbol{\xi}^{(i)})$, i.e., the ith row contains the values of the orthogonal polynomial basis Ψ_j evaluated at the ith sample point $\boldsymbol{\xi}^{(i)}$, and $\boldsymbol{\epsilon}$ is the vector of truncation errors. The spectral coefficients are computed by solving the following weighted least-squares minimization problem,

$$\min_{\boldsymbol{c}}\|\boldsymbol{W}^{\frac{1}{2}}(\mathbf{Q}-\boldsymbol{\psi}\boldsymbol{c})\|_2^2=\min_{c}(\mathbf{Q}-\boldsymbol{\psi}\boldsymbol{c})^\top\boldsymbol{W}(\mathbf{Q}-\boldsymbol{\psi}\boldsymbol{c}), \tag{7}$$

where $\boldsymbol{W}=(\boldsymbol{W}^{\frac{1}{2}})^\top\boldsymbol{W}^{\frac{1}{2}}$. The weighting matrix $\boldsymbol{W}^{\frac{1}{2}}$ is a diagonal positive-definite matrix, to be defined later. The solution of (7) results in the normal set of equations,

$$(\boldsymbol{\psi}^\top\boldsymbol{W}\boldsymbol{\psi})\hat{\boldsymbol{c}}=\boldsymbol{\psi}^\top\boldsymbol{W}\mathbf{Q}. \tag{8}$$

For system (8) to be well conditioned $q\gg P+1$. Evaluating the QoI $\overline{J}(\boldsymbol{\xi}^{(i)})$ at the q sample points is computationally expensive, and dominates the cost of the method. As mentioned in Sec. I, when the number of uncertain parameters m is large, the number of spectral coefficients P grows exponentially [Eq. (5) indicates $P+1\sim m^p$], leading to large computational cost, known as the curse of dimensionality.

The problem can be mitigated by enriching system (6) with gradient information. This method, called the sensitivity-enhanced gPC, or se-gPC, is presented in Ref. [21]. Differentiating Eq. (4) with respect to the kth random variable at the jth sample point we get,

$$\frac{\partial\overline{J}}{\partial\xi_k^{(j)}}=\sum_{i=0}^{P}c^{(i)}\frac{\partial\Psi_i}{\partial\xi_k^{(j)}}+\boldsymbol{\eta}_k(\xi^{(j)})\quad(j=1,\ldots,q). \tag{9}$$

For each random variable k, the block of q equations (9) can be written in matrix form as,

$$\frac{\partial\mathbf{Q}}{\partial\xi_k}=\frac{\partial\boldsymbol{\psi}}{\partial\xi_k}\boldsymbol{c}+\boldsymbol{\eta}_k\quad(k=1,\ldots,m), \tag{10}$$

where matrix $\frac{\partial\boldsymbol{\psi}}{\partial\xi_k}$ contains the gradients of the basis functions,

$$\frac{\partial\boldsymbol{\psi}}{\partial\xi_k}=\begin{bmatrix}\frac{\partial\Psi_0(\boldsymbol{\xi}^{(1)})}{\partial\xi_k^{(1)}} & \cdots & \frac{\partial\Psi_P(\boldsymbol{\xi}^{(1)})}{\partial\xi_k^{(1)}}\\ \vdots & \ddots & \vdots\\ \frac{\partial\Psi_0(\boldsymbol{\xi}^{(q)})}{\partial\xi_k^{(q)}} & \cdots & \frac{\partial\Psi_P(\boldsymbol{\xi}^{(q)})}{\partial\xi_k^{(q)}}\end{bmatrix}. \tag{11}$$

and vector $\frac{\partial\mathbf{Q}}{\partial\xi_k}$ stores the gradient of $\overline{J}$ with respect to the kth random parameter at the q sample points,

$$\frac{\partial\mathbf{Q}}{\partial\xi_k}=\left[\frac{\partial\overline{J}}{\partial\xi_k^{(1)}},\ldots,\frac{\partial\overline{J}}{\partial\xi_k^{(q)}}\right]^\top. \tag{12}$$

By stacking together $\mathbf{Q}$ and $\frac{\partial\mathbf{Q}}{\partial\xi_k}$, we define the following block column vector $\mathbf{G}\in\mathbb{R}^{(1+m)q\times1}$:

$$\mathbf{G}=\left[\mathbf{Q},\frac{\partial\mathbf{Q}}{\partial\xi_1},\ldots,\frac{\partial\mathbf{Q}}{\partial\xi_m}\right]^\top. \tag{13}$$

Similarly, by stacking together the measurement matrix $\boldsymbol{\psi}$ and its sensitivity $\frac{\partial\boldsymbol{\psi}}{\partial\xi}$, we define the following block matrix $\boldsymbol{\phi}\in\mathbb{R}^{(1+m)q\times(P+1)}$:

$$\boldsymbol{\phi}=\left[\boldsymbol{\psi},\frac{\partial\boldsymbol{\psi}}{\partial\xi_1},\ldots,\frac{\partial\boldsymbol{\psi}}{\partial\xi_m}\right]^\top. \tag{14}$$

We can therefore write the following $(1+m)\times q$ equations for the spectral coefficients $\boldsymbol{c}$:

$$\mathbf{G}=\boldsymbol{\phi}\boldsymbol{c}+\boldsymbol{\theta}. \tag{15}$$

As before, to compute the coefficients $\boldsymbol{c}$, we solve the following minimization problem:

$$\min_{c}\|\boldsymbol{W}'^{\frac{1}{2}}(\mathbf{G}-\boldsymbol{\phi}\boldsymbol{c})\|_2^2=\min_{c}(\mathbf{G}-\boldsymbol{\phi}\boldsymbol{c})^\top\boldsymbol{W}'(\mathbf{G}-\boldsymbol{\phi}\boldsymbol{c}), \tag{16}$$

where $\boldsymbol{W}'$ is a block diagonal weighting matrix, consisting of $1+m$ blocks $\boldsymbol{W}$. The solution $\hat{\boldsymbol{c}}$ is obtained via the normal equations,

$$(\boldsymbol{\phi}^\top\boldsymbol{W}'\boldsymbol{\phi})\hat{\boldsymbol{c}}=\boldsymbol{\phi}^\top\boldsymbol{W}'\mathbf{G}. \tag{17}$$

Notice the similarity between Eqs. (8) and (17). The weights $\boldsymbol{W}^{\frac{1}{2}}$ are computed with asymptotic sampling, a version of coherence sampling, see Ref. [40]. In this paper for simplicity (and without loss of generality) only Gaussian inputs are considered, and the weights can be computed analytically as,

$$W_{ii}^{\frac{1}{2}}(\boldsymbol{\xi})=exp(-\|\boldsymbol{\xi}\|^2/4). \tag{18}$$

For more details on the weights calculation and for extension to other input distributions, see Ref. [40].

To avoid large values of q, and thus keep the computational cost low, it is important to sample the QoI effectively. Different algorithms to sample the stochastic space are presented in Ref. [17]. In this paper, we apply QR decomposition. This is a greedy algorithm that maximizes the determinant of a matrix; in this sense it is a D-optimal design method, see Refs. [17,41,42]. The process is as follows: A large pool of q random sample points is generated (from the prescribed probability density functions) and the measurement matrix $\boldsymbol{\psi}$ is formed. The question is how to select a subset of at least $P+1$ points from this large pool. To this end, we multiply Eq. (6) from the left with the row selection matrix $\boldsymbol{\mathcal{P}}\in\mathbb{R}^{(P+1)\times q}$ and we get,

$$\boldsymbol{\mathcal{P}}\mathbf{Q}=\boldsymbol{\mathcal{P}}\boldsymbol{\psi}\boldsymbol{c}. \tag{19}$$

At each row of $\boldsymbol{\mathcal{P}}$ all elements are 0, except the element at the column that corresponds to the selected sampling point,

which takes the value of 1. In D-optimal experiment design, $\mathcal{P}$ is found as a solution to the following maximization problem:

$$\mathcal{P} = \underset{\boldsymbol{P}}{\operatorname{argmax}} \, |\det(\mathcal{P}\boldsymbol{W}^{1/2}\boldsymbol{\psi})|, \tag{20}$$

where det() denotes the determinant of a matrix. The solution to this problem is given via the pivoted QR decomposition,

$$(\boldsymbol{W}^{\frac{1}{2}}\boldsymbol{\psi})^{\top}\mathcal{P} = \boldsymbol{QR}. \tag{21}$$

The index matrix $\mathcal{P}$ is chosen so that the diagonal elements r_{ii} of $\boldsymbol{R}$ are ranked in descending magnitude $|r_{11}| \geqslant |r_{22}| \geqslant \cdots \geqslant |r_{ii}|$.

Since each sample point offers $1+m$ equations, at least $\frac{P+1}{1+m}$ samples with the highest r_{ii} scores are retained. Thus sensitivity enhancement reduces the computational cost compared to standard gPC by a factor m at the cost an adjoint evaluation at each sample point.

We could have applied the same approach to system (15) directly. However, applying QR decomposition to matrix $(\boldsymbol{W}^{\frac{1}{2}}\boldsymbol{\psi})^{\top}$ and computing at these points the QoI and its gradient is preferable compared to QR decomposition of the weighted augmented matrix $(\boldsymbol{W}'^{\frac{1}{2}}\boldsymbol{\phi})^{\top}$, see Ref. [21] for a comparison between the two approaches.

III. ADJOINT SENSITIVITY ANALYSIS OF CHAOTIC SYSTEMS

In this section we present a method for the computation of sensitivities of time-average quantities of chaotic systems to multiple parameters. To this end, we derive the adjoint version of the shadowing harmonic operator introduced in Ref. [39].

The goal of the LSS is to find a shadowing trajectory at $\boldsymbol{s}+d\boldsymbol{s}$ that stays in close proximity to (i.e., shadows) the reference trajectory at $\boldsymbol{s}$. If the underlying system is uniformly hyperbolic, the shadowing trajectory is guaranteed to exist. To achieve this goal, LSS solves the following minimization problem, see Ref. [32]:

$$\min_{\boldsymbol{v},\eta} \frac{1}{2}\int_0^T \|\boldsymbol{v}(t)\|^2 dt \; s.t. \tag{22a}$$

$$\frac{d\boldsymbol{v}}{dt} = \frac{\partial \boldsymbol{f}}{\partial \boldsymbol{u}}\boldsymbol{v} + \frac{\partial \boldsymbol{f}}{\partial \boldsymbol{s}} + \eta(t)\boldsymbol{f} \tag{22b}$$

$$\langle \boldsymbol{f}(\boldsymbol{u};\boldsymbol{s})\boldsymbol{v}(\boldsymbol{u};\boldsymbol{s})\rangle = 0, \tag{22c}$$

where $\boldsymbol{v}(t) = \frac{d\boldsymbol{u}(\tau(t);\boldsymbol{s})}{d\boldsymbol{s}}$ is the sensitivity of the solution $\boldsymbol{u}(t;\boldsymbol{s})$ to a change $\delta\boldsymbol{s}$ of $\boldsymbol{s}$, $\eta(t) = \frac{d}{d\boldsymbol{s}}(\frac{d\tau}{dt})$ is the time dilation, while (22c) denotes the orthogonality between the vectors $\boldsymbol{f}(\boldsymbol{u};\boldsymbol{s})$ and $\boldsymbol{v}(\boldsymbol{u};\boldsymbol{s})$ at each point along the trajectory. The gradient $\frac{d\bar{J}}{d\boldsymbol{s}}$ is then given by the following expression:

$$\frac{d\bar{J}}{d\boldsymbol{s}} = \frac{1}{T}\int_0^T \frac{\partial J}{\partial \boldsymbol{u}}\boldsymbol{v} + \frac{\partial J}{\partial \boldsymbol{s}} + \eta(t)(J-\bar{J})dt. \tag{23}$$

The solution of (22) has shown to produce accurate sensitivities [27–29,35].

In Ref. [39] the shadowing operator was formulated in the frequency domain. The key idea is to replace the minimization (22a) with the periodicity condition, yielding the following set of equations:

$$\frac{d\boldsymbol{v}}{dt} = \frac{\partial \boldsymbol{f}}{\partial \boldsymbol{u}}\boldsymbol{v} + \frac{\partial \boldsymbol{f}}{\partial \boldsymbol{s}} + \eta(t)\boldsymbol{f} \tag{24a}$$

$$\langle \boldsymbol{f}(\boldsymbol{u};\boldsymbol{s})\boldsymbol{v}(\boldsymbol{u};\boldsymbol{s})\rangle = 0 \tag{24b}$$

$$\boldsymbol{v}(0) = \boldsymbol{v}(T). \tag{24c}$$

Closing the system using periodicity leads to a sensitivity error that initially decays at a rate $1/T$, followed by the asymptotic rate $1/\sqrt{T}$ (the latter dictated by the central limit theorem), see also Ref. [43]. Nevertheless, condition (24c) makes the adjoint problem well posed, leading to physically meaningful and accurate sensitivities, as will be shown later.

The contribution of the present paper with respect to Ref. [39] is that an adjoint approach is taken, since sensitivities with respect to a large number of parameters are required. To this end, a Lagrangian function is defined,

$$\mathcal{L} = \frac{d\bar{J}}{d\boldsymbol{s}} + \frac{1}{T}\int_0^T \lambda^{\top}\mathcal{R}_{\boldsymbol{v}}dt + \frac{1}{T}\int_0^T \mu\mathcal{R}_{\eta}dt, \tag{25}$$

where $\mathcal{R}_{\boldsymbol{v}} \in \mathbb{R}^{N_u}$ and $\mathcal{R}_{\eta} \in \mathbb{R}$ are the residuals of (24a) and (24b), while $\lambda \in \mathbb{R}^{N_u}$ and $\mu \in \mathbb{R}$ are the adjoint state variables. This is expanded as

$$\begin{aligned}\mathcal{L} = &\frac{1}{T}\int_0^T \frac{\partial J}{\partial \boldsymbol{u}}\boldsymbol{v} + \frac{\partial J}{\partial \boldsymbol{s}} + \eta(t)(J-\bar{J})dt \\ &+ \frac{1}{T}\int_0^T \lambda^{\top}\left(\frac{d\boldsymbol{v}}{dt} - \frac{\partial \boldsymbol{f}}{\partial \boldsymbol{u}}\boldsymbol{v} + \frac{\partial \boldsymbol{f}}{\partial \boldsymbol{s}} + \eta\boldsymbol{f}\right)dt \\ &+ \frac{1}{T}\int_0^T \mu(\boldsymbol{f}^{\top}\boldsymbol{v})dt,\end{aligned}$$

and using integration by parts,

$$\begin{aligned}\mathcal{L} = &\frac{1}{T}\int_0^T \left(-\frac{d\lambda^{\top}}{dt} - \frac{\partial \boldsymbol{f}}{\partial \boldsymbol{u}}\lambda^{\top} + \frac{\partial J}{\partial \boldsymbol{u}} + \mu\boldsymbol{f}^{\top}\right)\boldsymbol{v}dt \\ &+ \frac{1}{T}\int_0^T \eta(J-\bar{J}-\boldsymbol{f}^{\top}\lambda)dt + [\boldsymbol{v}^{\top}\lambda]_0^T \\ &+ \frac{1}{T}\int_0^T \left(\frac{\partial J}{\partial \boldsymbol{s}} - \lambda^{\top}\frac{\partial \boldsymbol{f}}{\partial \boldsymbol{s}}\right)dt.\end{aligned}$$

We seek to make the Lagrangian independent of $\boldsymbol{v}(t)$ and $\eta(t)$. This is achieved by solving the following field adjoint equations:

$$\frac{d\lambda}{dt} = -\left(\frac{\partial \boldsymbol{f}}{\partial \boldsymbol{u}}\right)^{\top}\lambda + \frac{\partial J}{\partial \boldsymbol{u}} + \mu\boldsymbol{f} \tag{26a}$$

$$\boldsymbol{f}^{\top}\lambda = J - \bar{J} \tag{26b}$$

$$\lambda(0) = \lambda(T). \tag{26c}$$

The gradients can be computed from

$$\frac{d\bar{J}}{d\boldsymbol{s}} = \frac{1}{T}\int_0^T \left(\frac{\partial J}{\partial \boldsymbol{s}} - \lambda^{\top}\frac{\partial \boldsymbol{f}}{\partial \boldsymbol{s}}\right)dt. \tag{27}$$

Notice that (26a) is similar to (22b); the difference is that the transpose of the Jacobean is used and the time dilation term $\eta\boldsymbol{f}$ is replaced by the adjoint term $\mu\boldsymbol{f}$. The adjoint normality constraint (26b) has as forcing the residual $J-\bar{J}$. Note also that the periodicity condition (24c) for $\boldsymbol{v}$ extends also to λ, see (26c).

The above equations can be formulated in the frequency domain by expanding $\lambda(t)$ and $\mu(t)$ in Fourier series as

$$\lambda(t) = \sum_{k=-\ell}^{\ell} \hat{\lambda}_k e^{ik\omega_0 t}, \ \mu(t) = \sum_{k=-\ell}^{\ell} \hat{\mu}_k e^{ik\omega_0 t}, \tag{28}$$

where $\hat{\lambda}_k$, $\hat{\mu}_k$ are the Fourier coefficients and $\omega_0 = \frac{2\pi}{T}$ is the fundamental frequency. The index $k \in [-\ell, \ell]$ denotes the harmonics with frequencies $\omega_k = k\omega_0$. Introducing expansions (28) into (26a) and (26b), the system that yields the Fourier coefficients is written in compact form as

$$ik\omega_0 \mathcal{I}_u \begin{bmatrix} \hat{\lambda}_k \\ \hat{\mu}_k \end{bmatrix} + \sum_{l=-\ell}^{\ell} T_{k-l} \begin{bmatrix} \hat{\lambda}_l \\ \hat{\mu}_l \end{bmatrix} = \begin{bmatrix} \widehat{\frac{dJ}{du}}_k \\ \hat{f}_k - \overline{J} \end{bmatrix}, \tag{29}$$

where

$$\mathcal{I}_u = \begin{bmatrix} \mathcal{I}_{N_u} & 0 \\ 0 & 0 \end{bmatrix}, T_m = \begin{bmatrix} \left(-\widehat{\frac{\partial f}{\partial u}}\right)_m^\top & \hat{f}_m \\ \hat{f}_m^\top & 0 \end{bmatrix}. \tag{30}$$

We define the block diagonal matrix,

$$\mathcal{T}(T_m) = \begin{bmatrix} T_0 & T_{-1} & \dots & T_{-\ell} & & & \\ T_1 & T_0 & T_{-1} & \dots & T_{-\ell} & & \\ & \ddots & \ddots & \ddots & \dots & \ddots & \\ T_\ell & \dots & T_1 & T_0 & T_{-1} & \dots & T_{-\ell} \\ & \dots & \ddots & \ddots & \ddots & \ddots & \dots \\ & & T_\ell & \dots & T_1 & T_0 & T_{-1} \\ & & & T_\ell & \dots & T_1 & T_0 \end{bmatrix}, \tag{31}$$

which is a block Toeplitz matrix, because each diagonal has the same block. Using $\mathcal{T}(T_m)$, system (29) can be written in matrix form as

$$[\mathcal{D} - \mathcal{T}(T_m)]\widehat{\mathbf{\Lambda}} = \widehat{\mathcal{R}}, \tag{32}$$

where $\mathcal{D} = \text{diag}[\mathcal{D}_{-q}, \dots, \mathcal{D}_0, \dots, \mathcal{D}_q]$ is a block diagonal matrix with $\mathcal{D}_k = ik\omega_0 \mathcal{I}_u$, $\widehat{\mathcal{R}} = [\widehat{\mathcal{R}}_{-q}, \dots, \widehat{\mathcal{R}}_0, \dots, \widehat{\mathcal{R}}_q]^\top$ with $\widehat{\mathcal{R}}_k = [\widehat{\frac{dJ}{du}}_k, \hat{J}_k - \overline{J}]^\top$, and $\widehat{\mathbf{\Lambda}} = [\widehat{\Lambda}_{-q}, \dots, \widehat{\Lambda}_0, \dots, \widehat{\Lambda}_q]^\top$, where $\widehat{\Lambda}_k = [\hat{\lambda}_k, \hat{\mu}_k]^\top$. Matrix $\mathcal{H} = \mathcal{D} - \mathcal{T}(T_m)$ is also known as a Hill matrix.

Defining the adjoint shadowing harmonic operator as

$$\mathcal{A} = [\mathcal{D} - \mathcal{T}(T_m)]^{-1}, \tag{33}$$

the solution of system (32) can be written symbolically as

$$\widehat{\mathbf{\Lambda}} = \mathcal{A}\widehat{\mathcal{R}}. \tag{34}$$

The adjoint operator $\mathcal{A}$ maps the forcing $\widehat{\mathcal{R}}$ to the vector $\widehat{\mathbf{\Lambda}}$ that contains the unknown Fourier coefficients of the adjoint variables. More details can be found in Refs. [39,44,45].

We do not directly compute the adjoint shadowing operator $\mathcal{A}$. Instead we apply LU decomposition to the Hill matrix $\mathcal{H} = \mathcal{D} - \mathcal{T}(T_m)$ and find $\widehat{\mathbf{\Lambda}}$ by forward and backward substitution.

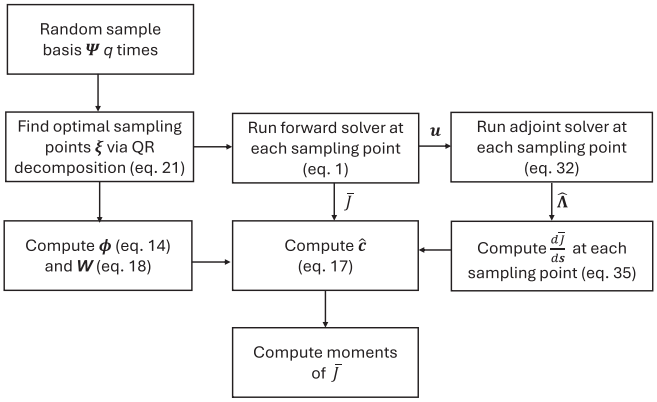

FIG. 1. Block diagram of the proposed UQ method. Arrows denote flow of information between blocks.

The gradients can then be computed from

$$\frac{d\overline{J}}{ds} = \left.\widehat{\frac{\partial J}{\partial s}}\right|_0 - \sum_{k=-\ell}^{\ell} \hat{\lambda}_k^\top \left.\widehat{\frac{\partial f}{\partial s}}\right|_{-k}, \tag{35}$$

which is the equivalent of (27) in Fourier space.

The cost of solving system (32) is independent of the number of parameters and thus the adjoint formulation can provide the sensitivities of time-average quantities of chaotic systems is a single step. This information is used to augment the se-gPC system as explained in the previous section.

We close this section with the block diagram shown in Fig. 1. The diagram presents the different components of the algorithm, as described in Secs. II and III, and how they are connected together.

IV. APPLICATION TO THE KURAMOTO-SIVASHINSKY SYSTEM

The aforementioned methodology is now applied to the forced Kuramoto-Sivashinsky (KS) equation,

$$u_t + uu_x + u_{xx} + u_{xxxx} = \phi(x), \tag{36}$$

where $x \in [0, L]$ and boundary conditions $u(0,t) = u(L,t) = 0$ and $u_x(0,t) = u_x(L,t) = 0$. Two QoIs are defined,

$$\overline{J^{(1)}} = \frac{1}{TL}\int_0^T \int_0^L J^{(1)}(x,t)dxdt,$$
$$\overline{J^{(2)}} = \frac{1}{TL}\int_0^T \int_0^L J^{(2)}(x,t)dxdt, \tag{37}$$

where $J^{(1)}(x,t) = u$ and $J^{(2)}(x,t) = u^2$, that represent time- and space-average values of the state and its energy. The KS equation was discretized in space using second-order central finite differences and integrated with a variable time step Runge-Kutta method. We take $L = 128$ that results in chaotic behavior. The state $u(x,t)$ was stored every $dt = 0.1$ time units and used as input to the adjoint system. The first 1000 time units were discarded to ensure that the system

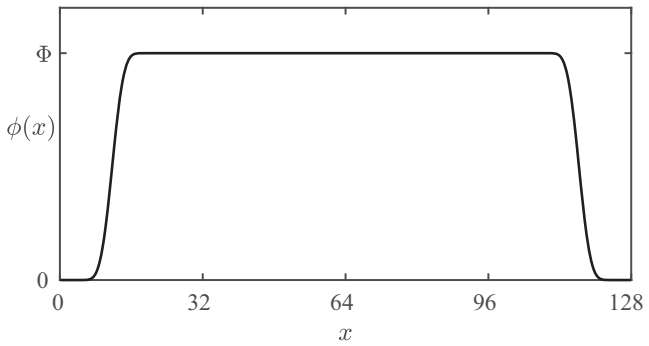

FIG. 2. Bell-shaped profile $\phi(x)$ with amplitude Φ.

has reached a chaotic attractor. The next $T = 100$ units were considered as the time horizon for the UQ analysis.

We first consider the bell-shaped forcing distribution $\phi(x)$ shown in Fig. 2, where Φ denotes the forcing amplitude. The smooth profiles from $0 \to \Phi$ (close to the left boundary) and from $\Phi \to 0$ (close to the right boundary) are obtained using the error function, erf, see Ref. [46] for more details. This forcing is infinitely differentiable and satisfies both Dirichlet and Neumann boundary conditions.

The variations of $\overline{J^{(1)}}$ and $\overline{J^{(2)}}$ with respect to amplitude Φ are shown in Figs. 3(a) and 4(a), respectively. The sensitivities of these QoIs obtained using finite differences and the adjoint of the shadowing harmonic operator are shown in Figs. 3(b) and 4(b), respectively. To form the harmonic operator, we consider frequencies in the range $f \in [-0.3, 0.3]$

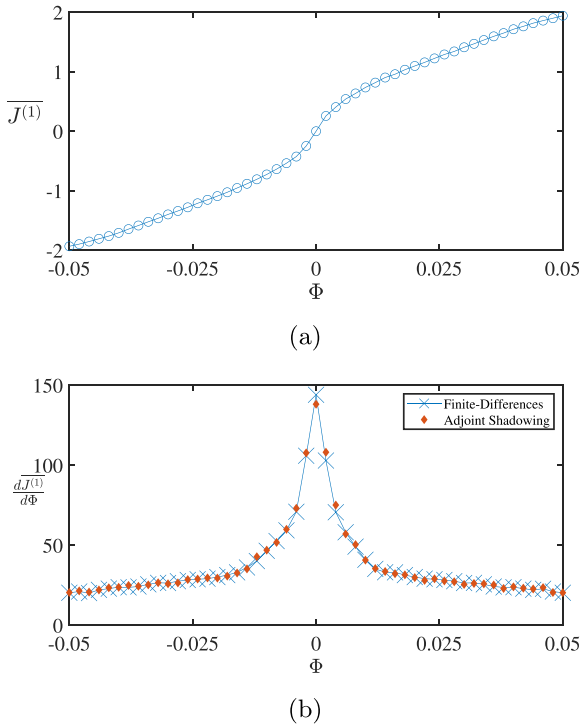

FIG. 3. Variation of (a) $\overline{J^{(1)}}$ with the forcing amplitude Φ and (b) sensitivity $\frac{d\overline{J^{(1)}}}{d\Phi}$ computed using the adjoint operator and finite differences. Results are averaged over 200 random initial conditions.

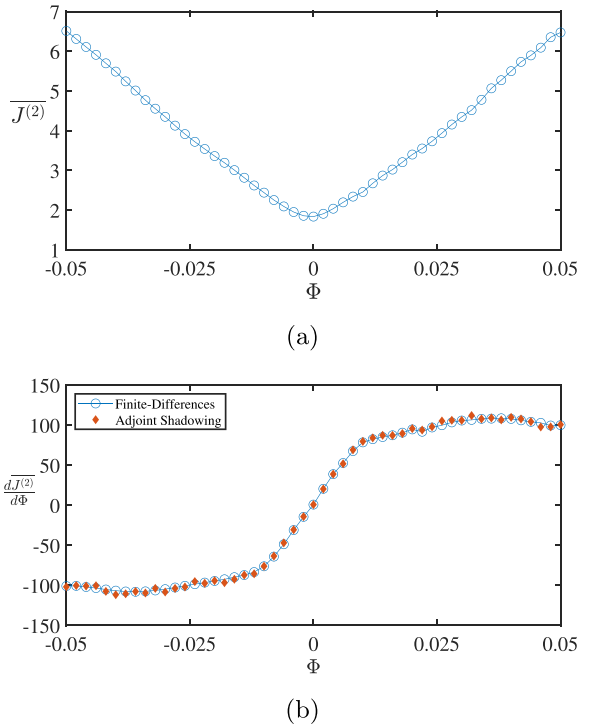

FIG. 4. Variation of (a) $\overline{J^{(2)}}$ with the forcing amplitude Φ and (b) sensitivity $\frac{d\overline{J^{(2)}}}{d\Phi}$ computed using the adjoint operator and finite differences. Results are averaged over 200 random initial conditions.

that captures the active frequency band of the unforced KS system, see Ref. [39]. Notice that the two approaches are in very good agreement for both QoIs. In this case, where the sensitivity with respect to a single parameter is considered, the adjoint shadowing operator does not provide any computational advantage over the standard shadowing harmonic operator, hence this test case is only used as a benchmark to evaluate the accuracy and computational implementation of the method.

Contour plots of the state and adjoint variables in the (t, x) plane for the unforced system, i.e., for $\phi(x) = 0$, are shown in Fig. 5. Notice that the adjoint variable $\lambda(x, t)$ does not have the same spatiotemporal streaky structure as the state variable $\boldsymbol{u}(x, t)$. This has been observed before in sensitivity analysis with shadowing method [35]. Similarly to the state $\boldsymbol{u}(x, t)$, the spatiotemporal structure of the adjoint state is characterized by high sensitivity to initial conditions. We now evaluate the effect of stochastic variation of Φ to $\overline{J^{(1)}}$ and $\overline{J^{(2)}}$ using the se-gPC method and the sensitivities produced with the adjoint shadowing operator to augment the least-squares system. We assume that Φ follows Gaussian distribution with $\Phi \sim \mathcal{N}(0, \sigma)$, and $\sigma = 0.01$. The standard deviation σ is small, but the response of the chaotic system to even small values of Φ is large, as shown in Figs. 3(a) and 4(a). For example, within the range $\Phi \in [-3\sigma, +3\sigma]$, the value of $\overline{J^{(2)}}$ doubles and the sensitivity varies between -100 to $+100$; this suggests that the effect of Φ is strong. In the range of Φ values considered the system is chaotic. Larger forcing amplitudes were also tested, however, they result in forced oscillations with nonchaotic behavior.

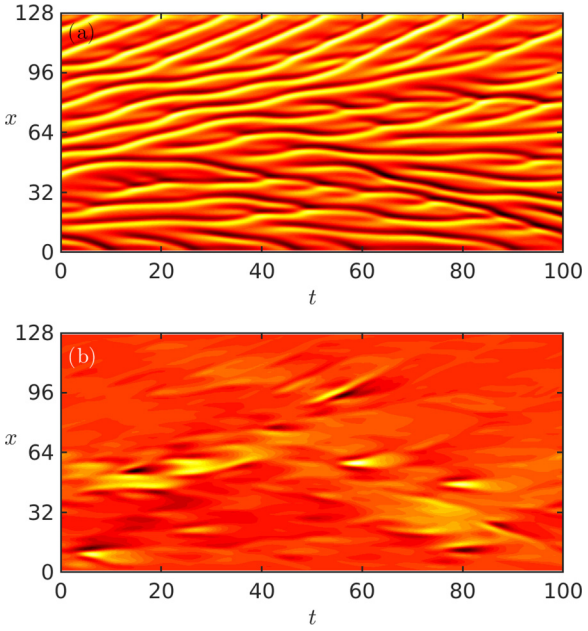

FIG. 5. Contour plots of the (a) state $\boldsymbol{u}(x,t)$ and (b) adjoint $\lambda(x,t)$ variables for the unforced system, $\phi = 0$. Results from a single realization with a random initial condition.

A Monte Carlo simulation with 5000 samples was performed and used as a benchmark to evaluate the accuracy of the se-gPC method. For a single stochastic variable ($m = 1$) and polynomial order $p = 1$, there are $P + 1 = 2$ spectral coefficients, while for $p = 2$ there are $P + 1 = 3$ coefficients. In the se-gPC we used $q = 4$ samples for $p = 1$, that were augmented with another four equations for the sensitivity of the QoI with respect to Φ. For $p = 2$, $q = 6$ samples were used, augmented with six additional equations for the sensitivity. We used more equations than the number of coefficients to account for the (small) variation of the sensitivities to initial conditions. The results for the mean and standard deviation of the QoIs are summarized in Table I, where se-gPC is compared with Monte Carlo (MC). There is very good agreement between the two methods. Errors in the standard deviation are less than 1.5% for $p = 1$ and less than 0.5% for $p = 2$ for both QoIs.

To better understand the effect of stochastic forcing $\phi(x)$, in Fig. 6 we plot the expectation of the time-average state, $\mathcal{E}[\overline{J^{(1)}(x)}]$, where $\overline{J^{(1)}(x)} = \frac{1}{T}\int_0^T J^{(1)}(x,t)dt = \frac{1}{T}\int_0^T u dt$, against x. We compare against the profile of the unforced system [$\phi(x) = 0$], where $\mathcal{E}[\overline{J^{(1)}(x)}] = \overline{J^{(1)}(x)}$. The

TABLE I. Comparison between Monte Carlo simulations with 5000 samples and se-gPC for the KS system. The stochastic input is $\Phi \sim \mathcal{N}(0, 0.01)$.

	se-gPC $p = 1$		se-gPC $p = 2$		Monte Carlo	
QoI	mean	std	mean	std	mean	std
$\overline{J^{(1)}}$	0.0196	0.6286	0.0196	0.6395	0.0195	0.6370
$\overline{J^{(2)}}$	2.3478	0.5251	2.3505	0.5174	2.3552	0.5192

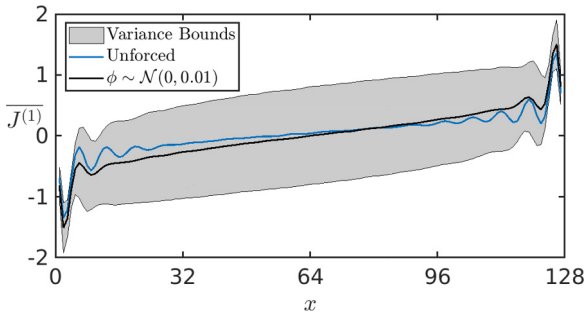

FIG. 6. $\mathcal{E}[\overline{J^{(1)}(x)}]$ for the unforced and forced KS system with $\Phi \sim \mathcal{N}(0, 0.01)$ for $T = 100$. Results are averaged over 1000 random initial conditions.

results are averaged over 1000 random initial conditions. It is interesting to notice that the stochastic forcing smoothes out the spatial oscillations of the time-average state of the unforced system. We also compute the standard deviation of $\overline{J^{(1)}(x)}$ across x, and we superimpose the extent of one standard deviation above and below the expectation (the area between the two boundaries is marked gray). The large spread indicates that the actual time-average $\overline{J^1(x)}$ oscillates wildly and can take values much larger than the expectation. Therefore the stochastic forcing drastically affects the output of the system. This explains why the standard deviation of $\overline{J^{(1)}}$ is much larger that the mean (expectation) in Table I.

V. MULTIDIMENSIONAL UNCERTAINTY FORCING

We now consider the stochastic forcing shown in Fig. 7, which is a continuous and differentiable profile that contains ten peaks and troughs. The local amplitudes Φ_i are the $m = 10$ independent stochastic variables considered. Such cases are usually found in control problems, where spatially complex forcing allows for more accurate control of the desired output quantities. The mean values of the localized forcing amplitudes are $\Phi_1 = 0.001$, $\Phi_2 = -0.001$, $\Phi_3 = 0.005$, $\Phi_4 = 0.002$, $\Phi_5 = 0.007$, $\Phi_6 = -0.003$, $\Phi_7 = -0.001$, $\Phi_8 = -0.002$, $\Phi_9 = 0.0005$, $\Phi_{10} = -0.002$. These

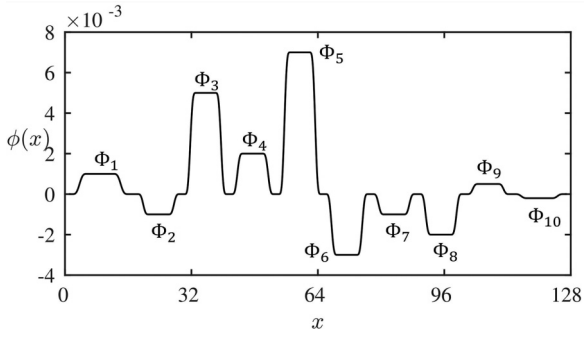

FIG. 7. Mean forcing $\phi(x)$ with $m = 10$ stochastic parameters, Φ_i ($i = 1, \ldots, m$). The forcing amplitudes are $\Phi_1 = 0.001$, $\Phi_2 = -0.001$, $\Phi_3 = 0.005$, $\Phi_4 = 0.002$, $\Phi_5 = 0.007$, $\Phi_6 = -0.003$, $\Phi_7 = -0.001$, $\Phi_8 = -0.002$, $\Phi_9 = 0.0005$, $\Phi_{10} = -0.002$.

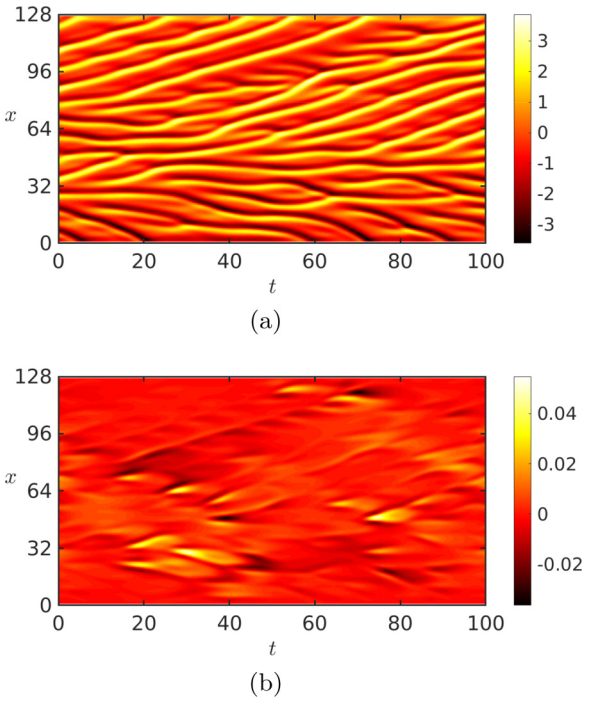

FIG. 8. Contour plots of (a) the state variable and (b) the adjoint variable for the KS system forced with the profile shown in Fig. 7. Results from a random initial condition.

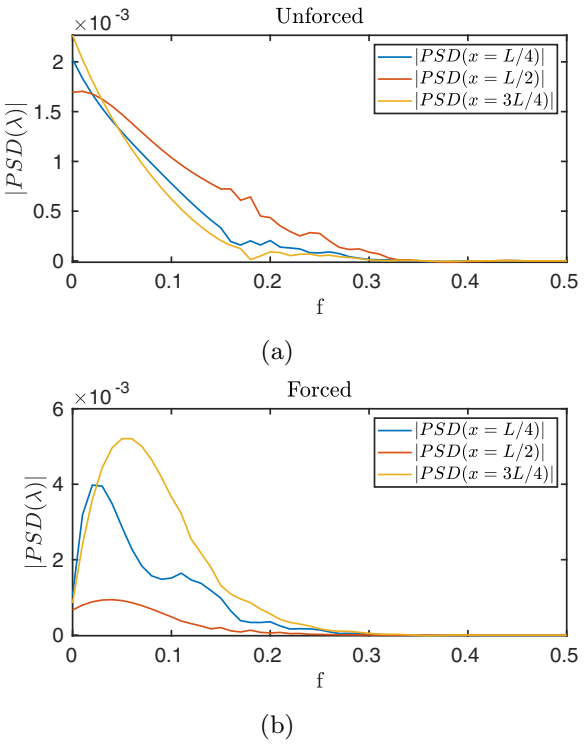

FIG. 9. Spectra of $\lambda(x,t)$ at $x = \frac{L}{4}, \frac{L}{2}$ and $\frac{3L}{4}$ for (a) the unforced and (b) the forced KS system.

values were selected arbitrarily, since the main objective of the section is to demonstrate the efficiency of the proposed computational approach to conduct UQ. The standard deviations are taken equal to 20% of the mean value, i.e., $\sigma_{\Phi_i} = |\Phi_i|/5$.

A. Characterization of the adjoint field

Contour plots of the direct and adjoint solutions at the mean values of Φ are shown in Fig. 8. Again the two solutions do not follow a similar structure. The adjoint variable $\lambda(x,t)$ shown in Fig. 8(b) maintains small values close to zero, but displays intermittent behavior with random peaks and troughs that have relatively short time duration.

The spectra of $\lambda(x,t)$ at $x = \frac{L}{4}$, $\frac{L}{2}$, and $\frac{3L}{4}$ are shown in Fig. 9 for the unforced and forced systems. The spectra were computed with a time window of $T = 100$ and were smoothed with a fifth-order Savitzky-Golay convolution filter with five averaging windows. For the unforced system, the spectra are very similar at the three locations. However, for the forced system the PSD values are larger and vary significantly between the locations due to the spatially varying forcing profile. The lower frequencies are also damped.

The accuracy of the adjoint shadowing harmonic operator is assessed in Fig. 10. The values of the $m = 10$ sensitivities computed by the adjoint operator are compared against reference finite difference results. To evaluate the reference results we varied each Φ_i separately and averaged over 100 initial conditions (we performed in total 1000 simulations with random initial conditions for all Φ_i's). The results for the adjoint shadowing operator were averaged over 100 random initial conditions. It is clear from the figure that the adjoint approach computes accurate sensitivities that are in very good agreement with finite differences for both $\overline{J^{(1)}}$ and $\overline{J^{(2)}}$.

B. Uncertainty quantification with se-gPC

We now proceed to conduct UQ with se-gPC; the independent stochastic variables are the $m = 10$ amplitudes Φ_i, as already mentioned. We first check if the system maintains its chaotic behavior with the stochastic forcing. To this end, the system was integrated for 2000 random Φ_i inputs over a time horizon of $T = 200$ and random initial conditions for each input. The Lyapunov exponents were computed for each realization using the methodology presented in Ref. [47]; the maximum exponent $\lambda_{\max}$ is shown in Fig. 11. For all realizations the forced system maintained its chaotic behavior, with a

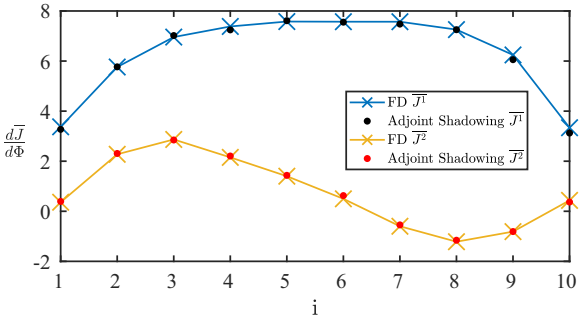

FIG. 10. Comparison of the sensitivities of $\overline{J^{(1)}}$ and $\overline{J^{(2)}}$ with respect to the amplitudes Φ_i computed using finite differences and the adjoint shadowing operator. Results are averaged over 100 initial conditions for the adjoint shadowing operator.

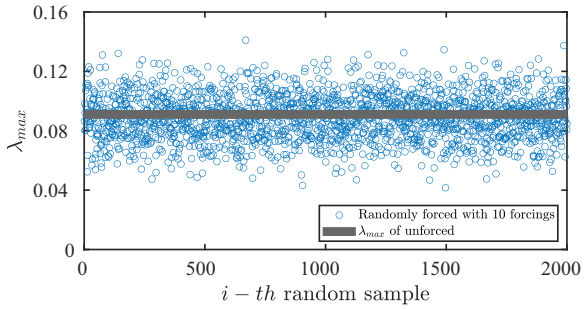

FIG. 11. Maximum Lyapunov exponent λ_{max} for 2000 realizations of $m = 10$ stochastic variables.

maximum Lyapunov exponent that fluctuates around the value of the unforced system (solid black line). For all systems it was observed that $\lambda_{\max} > 0.04$.

In Fig. 12, the convergence rates of the mean and standard deviation of $\overline{J^{(1)}}$ against the number of evaluations required by se-gPC, standard weighted least-squares [i.e., system (8)] and Smolyak quadrature are compared. It was assumed that one adjoint solution has the same cost as a direct solution (i.e., forward integration of the dynamical system). This is a realistic assumption for the KS system we consider, but generally the cost of obtaining the adjoint solution for a chaotic system is case dependent. In the plot, one adjoint or one forward solution is considered as a single evaluation. The errors are computed with respect to Monte Carlo with 10000 samples. The plot was obtained with $p = 2$, where Smolyak quadrature requires $(m + 1)(2m + 1) = 231$ evaluations. It is clear that the se-gPC outperforms the other two approaches, providing a very accurate estimation of the mean and the standard deviation with only 40 evaluations (this corresponds to 20 samples, with $1 + m = 11$ equations for each sample, in total 220 equations).

The corresponding plot for $\overline{J^{(2)}}$ is shown in Fig. 13. Once again, se-gPC coupled with the adjoint shadowing operator offers a significant computational advantage compared to other approaches. In practice this allows for the efficient

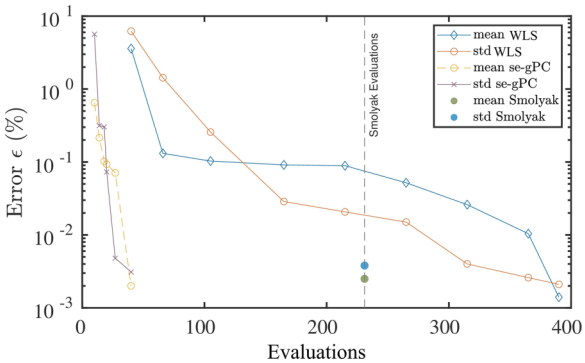

FIG. 12. Convergence rates of mean and standard deviation of $\overline{J^{(1)}}$ against number of evaluations computed with WLS, Smolyak quadrature and se-gPC for $p = 2$. The stochastic input is shown in Fig. 7.

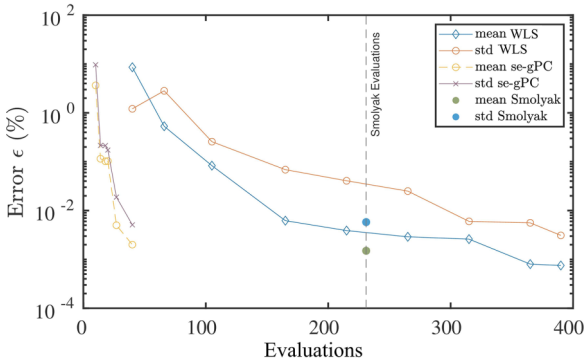

FIG. 13. Convergence rates of mean and standard deviation of $\overline{J^{(2)}}$ against number of evaluations computed with WLS, Smolyak quadrature and se-gPC for $p = 2$. The stochastic input is shown in Fig. 7.

quantification of uncertain input variables on the time-average quantities of chaotic systems.

VI. CONCLUSIONS

We propose a framework for efficient uncertainty quantification of time-average quantities of chaotic systems. We derive the adjoint version of the shadowing harmonic operator for sensitivity analysis of chaotic systems in the frequency domain. We subsequently employ the adjoint to compute the sensitivities of the QoI with respect to all uncertain variables and use this information to enrich the weighted least-squares system from which the spectral coefficients of polynomial expansion are computed. The adjoint formulation provides all the required sensitivities in a single step, thus significantly increasing the computational efficiency of the method. The sampling points to integrate the dynamical system are obtained by the QR decomposition of an appropriate weighted matrix. The computational cost of the method is independent of the number of stochastic variables for polynomial order $p = 1$.

The adjoint formulation was applied to the Kuramoto-Sivashinsky equation and found to produce accurate sensitivities with respect to the amplitude of bell-shaped forcing. When these sensitivities were used to augment gPC, the resulting first and second moments computed matched excellently with Monte Carlo results. We then tested the method on a stochastically forced system with ten independent input variables that determined the actual shape of the forcing. The adjoint was found to produce sensitivities that are in excellent agreement with finite differences and the se-gPC outperformed other UQ methods. These features make the proposed method a promising candidate for application to chaotic systems with a large number of stochastic inputs.

ACKNOWLEDGMENTS

K.D.K. acknowledges the financial support of the President's Scholarship Award from Imperial College London. The second author is supported by EPSRC Grants No. EP/X017273/1 and No. EP/W001748/1.

[1] E. Begoli, T. Bhattacharya, and D. Kusnezov, Nature Mach. Intell. **1**, 20 (2019).
[2] R. Ghanem and P. D. Spanos, J. Appl. Mech. **57**, 197 (1990).
[3] O. P. L. Maitre and O. M. Knio, *Spectral Methods for Uncertainty Quantification* (Springer, Dordrecht, 2010).
[4] M. Chatzimanolakis, K.-D. Kantarakias, V. Asouti, and K. Giannakoglou, Comput. Meth. Appl. Mech. Eng. **348**, 207 (2019).
[5] D. Xiu and G. E. Karniadakis, SIAM J. Sci. Comput. **24**, 619 (2002).
[6] S. A. Smolyak, Sov. Math. Dokl. **4**, 240 (1963).
[7] G. Blatman and B. Sudret, J. Comput. Phys. **230**, 2345 (2011).
[8] J.-C. Chassaing, D. Lucor, and J. Trégon, J. Sound Vib. **331**, 394 (2012).
[9] D. Schiavazzi, A. Doostan, G. Iaccarino, and A. Marsden, Comput. Meth. Appl. Mech. Eng. **314**, 196 (2017).
[10] B. A. Jones and A. Doostan, Adv. Space Res. **52**, 1860 (2013).
[11] Y. Che and C. Cheng, Chaos, Solitons Fractals **116**, 208 (2018).
[12] R. Bhusal and K. Subbarao, J. Comput. Nonlinear Dyn. **14** (2019).
[13] A. Abdulle and G. Garegnani, Stat. Comput. **30**, 907 (2020).
[14] K. D. Kantarakias, K. Shawki, and G. Papadakis, Phys. Rev. E **101**, 022223 (2020).
[15] K. D. Kantarakias and G. Papadakis, Algorithms **13**, 90 (2020).
[16] G. Blatman and B. Sudret, C. R. Mec. **336**, 518 (2008).
[17] M. Hadigol and A. Doostan, Comput. Methods Appl. Mech. Eng. **332**, 382 (2018).
[18] S. Oladyshkin and W. Nowak, Reliab. Eng. Syst. Saf. **106**, 179 (2012).
[19] E. Torre, S. Marelli, P. Embrechts, and B. Sudret, J. Comput. Phys. **388**, 601 (2019).
[20] R. Ahlfeld, B. Belkouchi, and F. Montomoli, J. Comput. Phys. **320**, 1 (2016).
[21] K. D. Kantarakias and G. Papadakis, J. Comput. Phys. **491**, 112377 (2023).
[22] J. Reuther, J. Alonso, M. Rimlinger, and A. Jameson, Comput. Fluids **28**, 675 (1999).
[23] K. Dems and Z. Mróz, Int. J. Solids Struct. **20**, 527 (1984).
[24] A. Sandu, D. N. Daescu, and G. R. Carmichael, Atmos. Environ. **37**, 5083 (2003).
[25] G. L. Eyink, T. W. N. Haine, and D. J. Lea, Nonlinearity **17**, 1867 (2004).
[26] D. J. Lea, M. R. Allen, and T. W. Haine, Tellus A: Dyn. Meteorol. Oceanogr. **52**, 523 (2000).
[27] Q. Wang, R. Hu, and P. Blonigan, J. Comput. Phys. **267**, 210 (2014).
[28] Q. Wang, SIAM J. Numer. Anal. **52**, 156 (2014).
[29] P. J. Blonigan and Q. Wang, Chaos, Solitons Fractals **64**, 16 (2014).
[30] S. Y. Pilyugin, *Shadowing in Dynamical Systems*, Lecture Notes in Mathematics, Vol. 1706 (Springer, Berlin, 1999).
[31] P. Holmes, J. L. Lumley, G. Berkooz, and C. W. Rowley, *Turbulence, Coherent Structures, Dynamical Systems and Symmetry*, 2nd ed. (Cambridge University Press, Cambridge, 2012).
[32] P. J. Blonigan and Q. Wang, J. Comput. Phys. **354**, 447 (2018).
[33] K. Shawki and G. Papadakis, J. Comput. Phys. **398**, 108861 (2019).
[34] A. Ni and Q. Wang, J. Comput. Phys. **347**, 56 (2017).
[35] P. J. Blonigan, J. Comput. Phys. **348**, 803 (2017).
[36] A. Ni, J. Fluid Mech. **863**, 644 (2019).
[37] A. Crisanti, M. H. Jensen, A. Vulpiani, and G. Paladin, Phys. Rev. Lett. **70**, 166 (1993).
[38] M. Hassanaly and V. Raman, Phys. Rev. Fluids **4**, 114608 (2019).
[39] K. D. Kantarakias and G. Papadakis, J. Comput. Phys. **474**, 111757 (2023).
[40] J. Hampton and A. Doostan, Comput. Meth. Appl. Mech. Eng. **290**, 73 (2015).
[41] A. Sommariva and M. Vianello, Comput. Math. Appl. **57**, 1324 (2009).
[42] K. Manohar, B. W. Brunton, J. N. Kutz, and S. L. Brunton, IEEE Control Syst. Mag. **38**, 63 (2018).
[43] D. Lasagna, A. Sharma, and J. Meyers, J. Comput. Phys. **391**, 119 (2019).
[44] N. M. Wereley, Ph.D. thesis, Massachusetts Institute of Technology, 1991, https://dspace.mit.edu/handle/1721.1/13761.
[45] A. Padovan, S. E. Otto, and C. W. Rowley, J. Fluid Mech. **900**, A14 (2020).
[46] J. Boyd, J. Sci. Comput. **29**, 1 (2006).
[47] L. Dieci, R. D. Russell, and E. S. Van Vleck, SIAM J. Numer. Anal. **34**, 402 (1997).